Superhyperfine interactions in inhomogeneously broadened paramagnetic centers observed via a hole-burned free induction decay

S. C. Drew, J. R. Pilbrow, P. J. Newman, and D. R. MacFarlane

Citation: The Journal of Chemical Physics **118**, 3148 (2003); doi: 10.1063/1.1535425
View online: http://dx.doi.org/10.1063/1.1535425
View Table of Contents: http://scitation.aip.org/content/aip/journal/jcp/118/7?ver=pdfcov
Published by the AIP Publishing

Superhyperfine interactions in inhomogeneously broadened paramagnetic centers observed via a hole-burned free induction decay

S. C. Drew[a] and J. R. Pilbrow
School of Physics and Materials Engineering, Monash University, Victoria 3800, Australia

P. J. Newman and D. R. MacFarlane
School of Chemistry, Monash University, Victoria 3800, Australia

(Received 18 June 2002; accepted 14 November 2002)

Superhyperfine interactions in inhomogeneously broadened paramagnetic centers are observed using a single high-turn-angle microwave pulse. The free induction signal that follows the hole-burning pulse exhibits oscillations that are distinct from the oscillatory free induction decay observable in some inhomogeneously broadened systems. It contains frequencies characteristic of the superhyperfine splittings, together with a zero frequency component. Experimental examples of the effect in both orientationally disordered (powdered) and structurally disordered (glassy) systems are presented and compared with the conceptually similar Fourier transform electron paramagnetic resonance detected nuclear magnetic resonance experiment, together with numerical simulations.
 [DOI: 10.1063/1.1535425]

I. INTRODUCTION

In electron paramagnetic resonance (EPR), the resonant absorption of microwave (mw) radiation by a paramagnetic system can be measured by monitoring the component of the magnetization in a plane transverse to an externally applied magnetic field, B_0. In Fourier transform EPR (FT-EPR), spectral information can be obtained by applying a mw pulse to rotate the magnetization into the transverse plane and then monitoring the electron Zeeman coherence in the form of a free-induction decay (FID), comprising a superposition of precession frequencies corresponding to the EPR level splittings. If the pulse is strong and short enough, then a large portion of the EPR spectrum can be excited at once and Fourier transformation of the FID signal yields all or part the EPR spectrum. For most solids, a short, nonselective mw pulse will result in the decay of the free-induction signal within the dead time of the mw detection system, due to inhomogeneous broadening of the EPR line. A selective mw pulse, however, burns a hole into an inhomogeneous line whose width approaches the homogeneous linewidth. The frequency selectivity of the pulse has the advantage of generating a FID that can be used to obtain high resolution field-swept pulsed-EPR spectra in both ordered[1] and disordered[2,3] systems.

It can also be used to detect the superhyperfine structure (shf) present in the spectrum in various ways (Fig. 1). Application of a mw pulse of appropriate duration and strength can influence electron polarization (EP), electron coherence (EC), and nuclear coherence (NC). A number of two-pulse experiments are possible which exploit each of these to measure electron-nuclear interactions. In a FT-EPR detected nuclear magnetic resonance (NMR) experiment[4] a nonselective $\pi/2$ pulse transfers the electron polarization pattern (holes) created by a selective pulse into EC in the form of a FID, which contains only a zero frequency component and the sublevel frequencies. (The FID following the second pulse contains only the frequencies of the holes, because all other EC excited by the short pulse decays within the spectrometer dead time.) A two-pulse method for studying nuclear coherences[5] utilizes the NC created by a selective (π) pulse, which is transferred into EC by a nonselective $\pi/2$ pulse at a later time T; the FID after the second pulse is measured at a fixed point as a function of T and contains modulations at the sublevel frequencies. Last, in the extended-time excitation scheme,[6] a nonselective π pulse refocuses the EC created by the long, weak pulse into an echo, whose intensity exhibits a beating between allowed and forbidden magnetic dipole transitions.

In the present case, we show that the long and weak mw pulse, alone, can be used to detect sublevel splittings in inhomogeneously broadened systems *via* the generation of beats in the hole-burned FID (HB-FID). This perhaps unexpected result is not related to the microwave-induced transitory oscillations discussed by Braunschweiler *et al.*,[7] where, interestingly, they suggested that large hyperfine interactions may distort the oscillatory FID. Hole-burning experiments in EPR are based upon optical hole-burning techniques. For example, the FT-EPR detected NMR experiment is the analog of the optical hole-burning technique of Nakanishi *et al.*,[8] where the FID exhibits beats arising from superhyperfine structure.

II. THEORY

The phenomenon cannot be adequately described using the extended-time-excitation concept because the linear regime approximation holds only for small nominal flip angles.[6,9] The present qualitative description considers the case of a simple $S=1/2$, $I=1/2$ four-level system and, given

[a]Present address: Center for Magnetic Resonance, The University of Queensland, Brisbane 4072, Australia; electronic mail: simon.drew@cmr.uq.edu.au

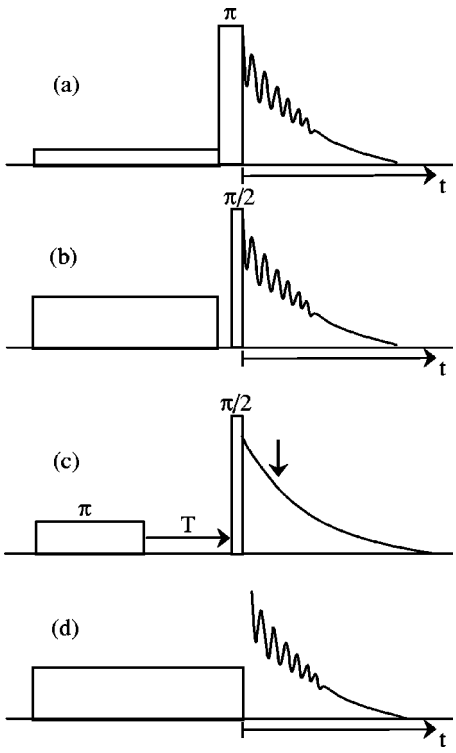

FIG. 1. Pulse schemes which employ a selective excitation pulse to observe superhyperfine interactions. (a) Extended-time excitation (EC); (b) FT-EPR detected NMR (EP); (c) low frequency nuclear coherences (NC); (d) quantum beat FID (EC).

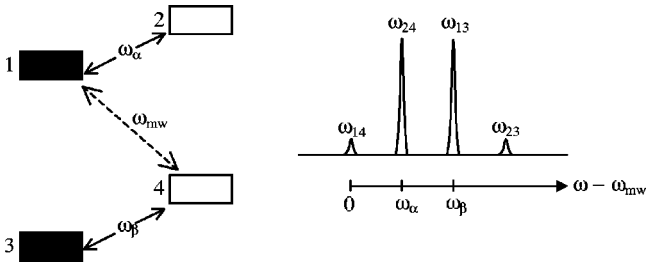

FIG. 2. Schematic of an $S=1/2$, $I=1/2$ system, showing changes in populations of the energy levels associated with the allowed transitions 1–3 and 2–4 by selective excitation of the forbidden transition 1–4 with a hole-burning mw pulse.

that a stand-alone hole-burning mw pulse represents the preparation part of the FT-EPR detected NMR experiment, we use similar concepts invoked in the latter[4,10,11] to explain the former. The key physical ideas will therefore only be briefly summarized.

The inhomogeneous line may be viewed as being comprised of a superposition of many spin packets differing only in their frequency offset.[4,10,12] The pulse has a bandwidth that is narrow enough to excite only a single transition in a given spin packet, so that within the inhomogeneous line there will exist only four spin packets with on-resonance transitions. For selective excitation, the effective rotation angle of the magnetization corresponding to each of the transitions is weighted by the transition moment. In particular, the effective flip angle for the forbidden transitions is given by[4,10]

$$\beta_f = \omega_1 t_p \sin\eta = \omega_1 t_p \sqrt{I_f}, \tag{1}$$

where ω_1 is the magnitude of the mw magnetic induction in angular frequency units, t_p is the length of the selective pulse, $I_f = \sin^2\eta$ is the transition probability of the forbidden transitions, and 2η is the angle between the nuclear quantization axes in the $m_s = \pm 1/2$ states. The effective flip angle for the allowed transitions is

$$\beta_a = \omega_1 t_p \cos\eta = \beta_f \sqrt{I_a/I_f}. \tag{2}$$

In the usual instance where $\beta_a \approx \pi/2$ for the generation of a FID following a $\pi/2$ pulse, the transverse magnetization (EC) corresponding to the forbidden transitions is small, by virtue of their small transition probability ($I_f/I_a \ll 1$). In the present instance, in order to observe the beats in the HB-FID, the mw pulse should be applied for a time long enough such that the magnetization due to on-resonance forbidden transitions has an effective flip angle close to $\beta_f = \pi$. Treating the levels involved in the forbidden transition as a virtual two-level system, the populations of the upper and lower electron spin manifolds are consequently equalized (Fig. 2). By inverting the magnetization of the on-resonance forbidden transition, the magnetization associated with the allowed transitions (of the same spin packet), with frequency offset ω_α and ω_β, is therefore indirectly brought into the transverse plane (EC). The magnetization associated with the other (off-resonance) forbidden transition of the same spin packet is unaffected. An analogous argument follows for the spin packet with the other forbidden transition on-resonance, except now the frequency offsets of the transverse magnetization are $-\omega_\alpha$, $-\omega_\beta$.

For the two spin packets with on-resonance allowed transitions, the effective flip angle $\beta_a \gg \beta_f$ so that the magnetization in this instance nutates many times in a plane perpendicular to ω_1 in the time t_p it takes to invert the levels of the on-resonant forbidden transition. Depending on the precise flip angle β_f and the ratio I_a/I_f, the final orientation of the magnetization vector of the on-resonant allowed transition may lie anywhere between its equilibrium position and inversion, so that it contributes a zero frequency component of variable magnitude depending on its measurable transverse component. Note that the off-resonant allowed transition within this spin packet is unaffected and that the off-resonant forbidden transitions make negligible contributions to the transverse magnetization due to the fact that $\beta_f \ll \beta_a$.

The coherently detected FID is therefore comprised of a dc component, together with the sublevel frequencies ω_α, ω_β. When there exist couplings with nuclei of spin $I > 1/2$, it is not possible to completely remove the dc frequency component by a judicious choice of t_p, since a single forbidden transition can only couple two allowed transitions. When one or more (generally inequivalent) nuclei are coupled to the paramagnetic spin, higher quantum transitions involving combination frequencies of the splitting due to each nucleus are possible. These involve spin flips of the electron together with nuclear spin-flips of more than one coupled nucleus; such multiple spin-flip transitions have smaller transition probabilities than single spin-flip transitions.

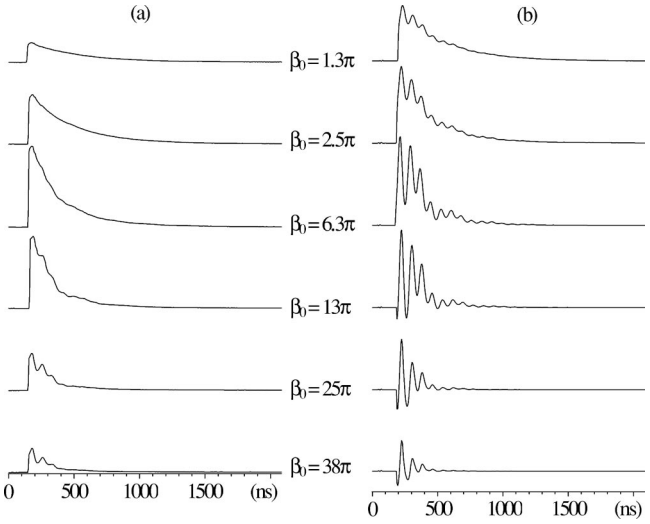

FIG. 3. Cu^{2+}-doped ZBLAN glass; $t_p = 2000$ ns, 9.7 GHz, 2.7 K, $B_0 = 3200$ G. (a) HB-FID; (b) FT-EPR detected NMR.

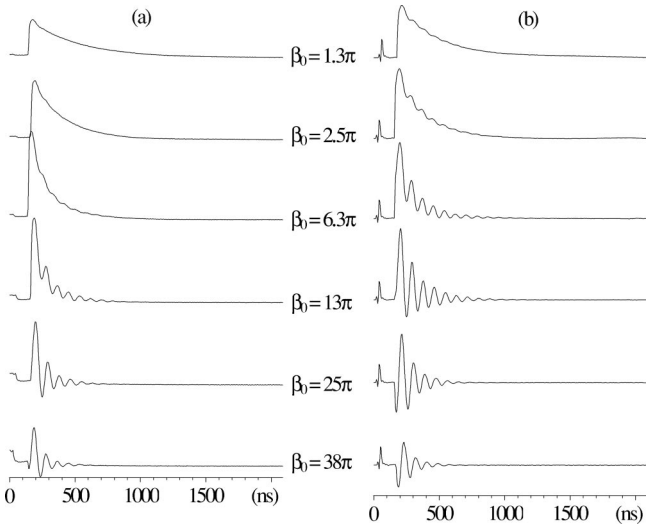

FIG. 4. Ce^{3+}-doped metaphosphate glass; $t_p = 2000$ ns, 9.7 GHz, 2.7 K, $B_0 = 7000$ G. (a) HB-FID; (b) FT-EPR detected NMR. The trailing edge of the preceding mw pulse can be seen in each.

III. EXPERIMENT

The ZBLAN glass samples were made within the School of Chemistry, Monash University as outlined in a previous publication.[13] The composition of the base glass by weight percent was: ZrF_4(53%), BaF_2(20%), LaF_3(4%), AlF_3(3%), NaF(20%). This was doped with 1000 ppm Cu^{2+}. The Metaphosphate glass sample was supplied by Dr. Don Ball (University of Capetown) and prepared by Professor G. A. Saunders and Dr. Richard Martin (University of Bath, UK). Its composition was $(Ce_2O_3)_{0.01}(Y_2O_3)_{0.19}(P_2O_5)_{0.80}$.

All spectra were obtained with a Bruker ESP380E FT spectrometer[2] equipped with a Bruker ER4118 X-band dielectric resonator, an Oxford Instruments CF 935 liquid helium cryostat and a 1 kW TWT amplifier. A LeCroy 9450A 300 MHz digital oscilloscope was used to record the transients. The main attenuator setting of the spectrometer was adjusted to optimize a Hahn echo using a 16 ns $\pi/2$ pulse. Using this setting, the power of the hole burning pulse was then varied using the level potentiometer of the mw channel. The FT-EPR detected NMR experiment used three mw channels, one for the selective pulse and two to carry out the phase-cycling sequence $(0,0)$-$(0,\pi)$, which removed the EC (including the HB-FID) created by the selective mw pulse. The signal was averaged over 2000 shots for each step of the phase cycle, while the HB-FID was averaged over 4000 shots. Time-domain spectra were apodized with a hanning window prior to fast Fourier transform (FFT) in order to counteract the influence of the decay of the FID.

IV. RESULTS

Figures 3 and 4 show the HB-FID following a 2 μs rectangular pulse for the Cu^{2+}-doped ZBLAN glass and the Ce^{3+}-doped metaphosphate glass, respectively, as a function of the mw power. For comparison, the FT-EPR detected NMR experiment is also shown at the same corresponding mw power and scale. Interactions due to weakly coupled matrix nuclei can be seen as indicated in Figs. 3 and 4. The nominal flip angle β_0 indicated next to each spectrum was estimated by comparing the applied mw field strength B_1 (measured with the transmitter monitor) with that required to optimize a primary echo using a $\pi/2$ pulse of 16 ns:

$$\beta_0 \simeq \theta_{p1} = \theta_{p2}\frac{(B_1)_{p1}t_{p1}}{(B_1)_{p2}t_{p2}} = 62.5\pi\frac{V_{p1}}{V_{p2}}, \tag{3}$$

where θ_{p1} is the turn angle of the selective mw pulse, $t_{p1} = 2000$ ns, $t_{p2} = 16$ ns, $\theta_{p2} = \pi/2$, and V is the voltage measured by the transmitter monitor. Clearly, the accuracy of the values obtained in this way are limited by the visual optimization of the primary echo and therefore the quoted nominal turn angles are only intended to be a rough guide. The frequency domain spectra (Figs. 5 and 6) were obtained using the Bruker WIN-EPR software by shifting the zero of time to remove the dead time, subtracting the unmodulated decay using a polynomial fit, apodizing with a hanning window function, zero-filling to 1024 points and taking a magnitude FFT.

An example of the HB-FID in an *orientationally* disordered system is given in Fig. 7, where the beats due to remote protons in polycrystalline γ-irradiated alanine can be seen superimposed upon the oscillatory FID. Here the nominal flip angle can easily be extracted from the number of transitory oscillations present in the FID.[7] An oscillatory FID cannot be seen in the glasses presumably because of the distributions of spin Hamiltonian interactions that result from the structural disorder.

V. NUMERICAL SIMULATIONS

As a model system, we consider the simplest case of a single crystal possessing an axial rotating frame Hamiltonian (neglecting nonsecular terms) and isotropic g tensor

$$\mathcal{H}_0 = (\omega_0 - \omega_{\mathrm{mw}})S_z + \omega_I I_z + AS_zI_z + BS_zI_x, \tag{4}$$

where $\omega_0 = g\beta_e B_0/\hbar$ is the electron Zeeman frequency, ω_{mw} the microwave frequency, and $\omega_I = -g_n\beta_n B_0/\hbar$ is the

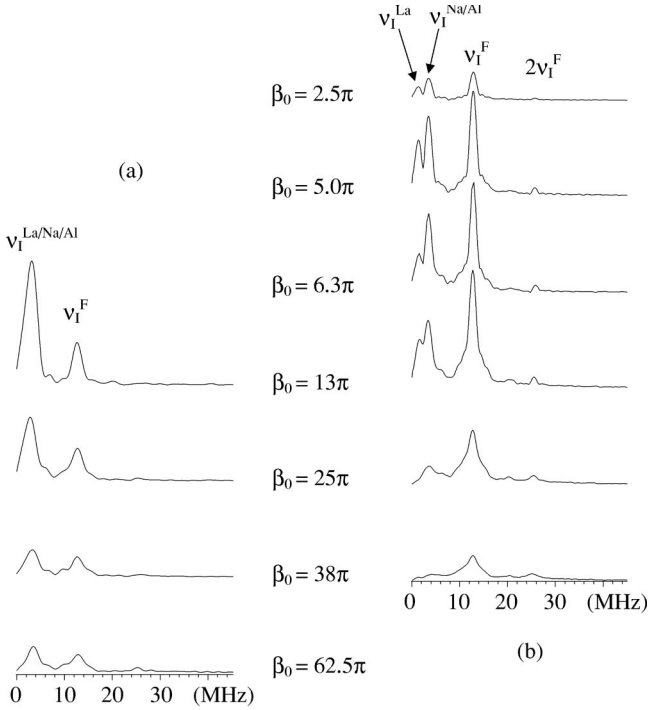

FIG. 5. Frequency domain (magnitude) spectra corresponding to the Cu^{2+}/ZBLAN system of Fig. 3. The scales in (a) and (b) are not comparable.

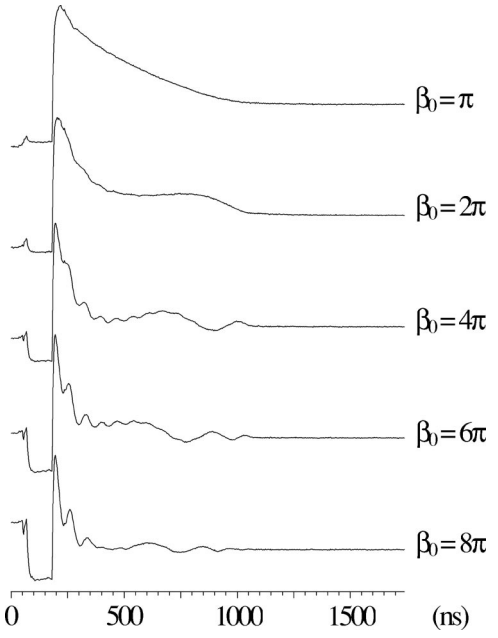

FIG. 7. HB-FID of γ-irradiated alanine powder (10^4 Gy) obtained from excitation at the central resonance of the EPR spectrum (of width $\approx$25 MHz); $t_p = 1000$ ns, $\omega_{mw} = 9.7$ GHz, 100 K. The quantum beats due to remote protons can be seen superimposed upon the oscillatory FID. The (arbitrary) high power attenuation settings were (from top to bottom) 33, 27, 21, 18, and 15 dB. The approximate value of β_0 was estimated from the number of transitory oscillations (Ref. 7).

nuclear Zeeman frequency. The secular and psuedosecular components of the hyperfine interaction are given by

$$A = T(3\cos^2\theta - 1) + a_{\text{iso}}, \tag{5}$$

$$B = 3T\cos\theta\sin\theta, \tag{6}$$

where

$$T = \left(\frac{\mu_0}{4\pi}\right)\frac{g g_n \beta_e \beta_n}{\hbar r^3} \tag{7}$$

is the dipolar coupling constant. Here θ defines the angle between the electron-nuclear axis and the static magnetic field, r is the electron-nuclear separation, and a_{iso} represents the isotropic hyperfine coupling strength. The hyperfine splittings are related to the coupling parameters via

$$\omega_\beta^\alpha = \left[\left(\frac{A}{2} \pm \omega_I\right)^2 + \left(\frac{B}{2}\right)^2\right]^{1/2} \tag{8}$$

and the allowed and forbidden transition probabilities are determined from

$$I_f^a = \frac{\left|\omega_I^2 - \frac{1}{4}(\omega_\alpha \mp \omega_\beta)^2\right|}{\omega_\alpha \omega_\beta}, \tag{9}$$

where meaningful values of $I_a, I_f \leqslant 1$ are only obtained for

$$\omega_\alpha + \omega_\beta \geqslant 2\omega_I \geqslant |\omega_\alpha - \omega_\beta|. \tag{10}$$

The same hypothetical parameters as used by Wacker and Schweiger are utilized,[4] namely a ratio $I_a/I_f = 100$ and nuclear frequencies of $\omega_\alpha = 8$ MHz, $\omega_\beta = 18$ MHz. Using Eqs. (8)–(10), this corresponds to hyperfine parameters of $A \approx 10.04$ MHz, $B \approx 2.095$ MHz, and $\omega_I \approx -12.95$ MHz and therefore weak hyperfine coupling ($|A| < 2|\omega_I|$).

The model system was simulated using the density operator approach with a home-written FORTRAN 90 program based upon exact solution of the Liouville equation. Computation of propagators of the form $U = e^{-i\mathbf{A}t}$ was accomplished using the eigenvalue-eigenvector decomposition of the $n \times n$ Hermitian matrix $\mathbf{A}$ and by noting that the exponential can be expressed in the following form:

$$e^{-i\mathbf{A}\mathbf{t}} = e^{-i(\mathbf{Z}\cdot\mathbf{\Lambda}\cdot\mathbf{Z}^\dagger)\mathbf{t}} = \mathbf{Z}\cdot\mathbf{e}^{-i\mathbf{\Lambda}\mathbf{t}}\cdot\mathbf{Z}^\dagger, \tag{11}$$

where the $n \times n$ matrix $\mathbf{Z} = (\mathbf{z}_1, \ldots, \mathbf{z}_n)$ contains the $n \times 1$ eigenvectors $\mathbf{z}_j$ of $\mathbf{A}$ and $\mathbf{\Lambda} = \text{diag}(\lambda_1, \ldots, \lambda_n)$ is a diagonal matrix containing the corresponding eigenvalues λ_j. In this

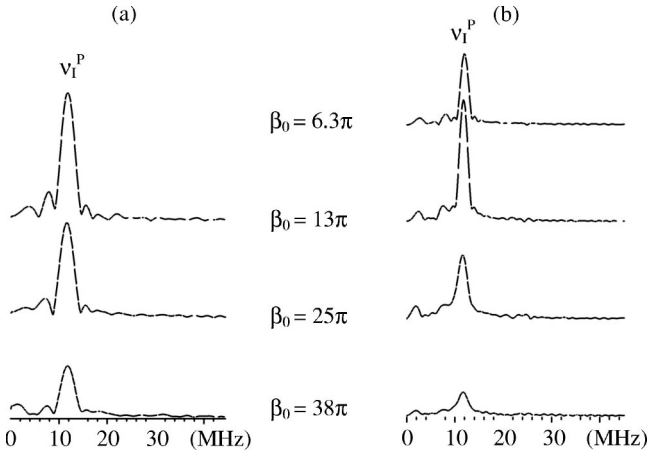

FIG. 6. Frequency domain spectra corresponding to the Ce^{3+} system of Fig. 4. The scales in (a) and (b) are not comparable.

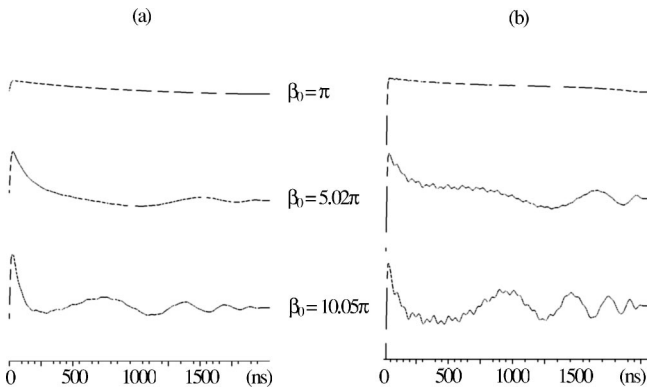

FIG. 8. Simulations of (a) HB-FID and (b) FT-EPR detected NMR experiments. Both (a) and (b) are drawn to the same scale. Simulation parameters: $g=2$, $A=10.04$ MHz, $B=2.095$ MHz, $\omega_I=-12.95$ MHz, $\Gamma_{\text{inh}}=25$ MHz, $t_{\text{sel}}=2\ \mu$s, $t_{\pi/2}=10$ ns.

form, the computation of the exponential is trivial because $\exp[\text{diag}(\lambda_1,...,\lambda_n)]=\text{diag}(\exp[\lambda_1],...,\exp[\lambda_n])$. Equation (11) can be verified term by term using a series expansion of the exponential.

Excitation at the center of a Gaussian inhomogeneous line with $\Gamma_{\text{inh}}=25$ MHz was assumed, the line shape being accounted for by using a weighted summation over all resonance frequency offsets, which was approximated by 500 point histogram in the range ± 3 standard deviations. The full width at half maximum, Γ_{inh}, of the Gaussian is related to the standard deviation $\Delta\omega$ by

$$\Delta\omega=\frac{\Gamma_{\text{inh}}}{\sqrt{2\ln 2}}. \tag{12}$$

A 2 μs rectangular mw pulse was assumed. For the FT-EPR detected NMR simulation, this was immediately followed by a nonselective 10 ns $\pi/2$ pulse together with a two-step phase-cycle $(0,0)-(0,\pi)$. To make the intensity of HB-FID simulation comparable, it was performed twice and its intensity accumulated. The data were output in a format suitable for analysis using the WIN-EPR/Xepr software.

The results are shown in Fig. 8 for three values of the nominal turn angles β_0 of the hole-burning pulse. In both experiments, a beat signal can be seen superimposed upon the transitory oscillations. The values $\beta_0=5.02\pi$ and $\beta_0=10.05\pi$ correspond to effective flip angles of $\beta_f=\pi/2$ and $\beta_f=\pi$, respectively. The latter represents the condition for the maximum population difference that can be created for the allowed transition sharing the common energy level and consequently for the maximum modulation depth of the FID in both (a) and (b). The modulation depth produced by observing the EC immediately following the HTA pulse is clearly much smaller than that obtained by observing the EP.

VI. DISCUSSION

The numerical simulations considered only the model system of a single crystal possessing an anisotropic hyperfine interaction and a large inhomogeneous linewidth. On the other hand, only superhyperfine interactions with very small anisotropy were observed in the experimental spectra of the disordered systems, since a large anisotropy leads to a strong orientational dependence of the beat frequency. This results in a decay of the free-induction signal within the spectrometer dead time due to destructive interference of the free precessional phase factors during orientational averaging. Thus, only interactions with weakly coupled remote matrix nuclei are expected, as is commonly the case in ESEEM of disordered systems, for example.[14] The strength of the beat signal for orientationally and structurally disordered systems will therefore depend on the weak couplings to a large number of remote nuclei.

Both the HB-FID and FT-EPR detected NMR experiments rely on inhomogeneous broadening of the EPR line. A frequency selective mw pulse excites on-resonance forbidden transitions, which indirectly alters the population difference of the allowed transitions that share a common energy level with forbidden ones. The ensuing FID contains precession signals at frequencies characteristic of shf interaction splittings. A zero frequency component will also be present due to the excitation of spin packets with on-resonance allowed transitions. It is expected that as ω_1 increases, those forbidden transitions with larger transition probabilities will have peaks approaching maximum intensity in the Fourier spectrum whilst those with smaller transition moments will still be increasing in height. Indeed, the intensity of the combination frequency peaks in Fig. 5(b) continues to increase relative to the single spin-flip transitions with larger mw powers.

In comparing the experimental FT spectra, is must be noted that different width window functions were chosen for the HB-FID and FT-EPR detected NMR experiments, in order to best enhance the data in each. Therefore, a comparison of their absolute intensities should not be attempted. However it is clear from the time domain data, whose intensities *are* comparable, that the strength of the beating in the HB-FID is relatively weak. In comparing relative peak intensities *within* each experiment, where the spectra are all drawn to the same scale, it is seen that an increase in mw power leads to a faster decay of the free induction signal and hence weaker, broader low-frequency features.

The use of a pulse $t_p \gtrsim T_M$, where T_M defines the phase memory time, means that transverse relaxation processes are active during the preparation pulse so that EC is already reduced at the start of the detection period. However the use of a shorter pulse requires a larger ω_1 to turn the forbidden magnetization by the same amount, which in turn leads to a shorter FID due to the increased excitation bandwidth. This makes identification of the low frequency modulations more difficult and there will exist an interplay between T_M, ω_1 and t_p for optimal sensitivity and selectivity. It may be in some instances that T_M is too short and I_f too small to even partially rotate the forbidden magnetization while maintaining an observable FID.

The qualitative description given in Sec. II suggests that for ideal selective excitation, the $\beta_f=\pi$ pulse in Fig. 2 may be interpreted as creating both a hole of depth I_a and a maximum measurable EC for the coupled allowed transitions; thus in the absence of relaxation, the signal from both the HB-FID and FT-EPR detected NMR should be comparable. Yet the numerical simulations neglect T_M and T_1 relaxation

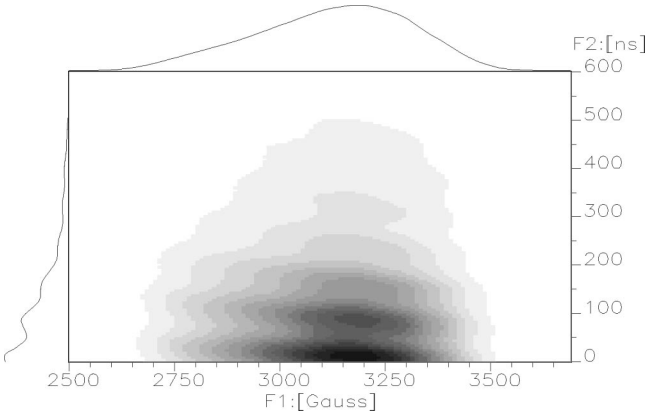

FIG. 9. Field dependence of the HB-FID time domain of the Cu^{2+}/ZBLAN at an arbitrary high power attenuator setting of 20 dB. A skyline projection along each axis is shown.

and still the modulations in the HB-FID are relatively quite weak. This may be attributed to the decay of the EC resulting from the finite excitation bandwidth $\Delta\omega$, the characteristic decay time being of the order $1/\Delta\omega$. The more complicated sinc-shaped excitation profile for the rectangular HTA pulse would also contribute unwanted off-resonance contributions in the form of the transitory oscillations and may also be expected to further reduce the transverse decay time.

Whereas the shape and depth of the holes will depend on the relative length of t_p and T_M, the decay of the EP is primarily determined by $T_1 > T_M$ and hence the FT-EPR detected NMR beat signal will always be stronger, as is seen in all experimental examples. In addition to higher sensitivity, it also possesses higher resolution because the linewidths in the FT spectra are narrower than in the HB-FID. This is most evident in Fig. 5(b), where the La^{139} peaks can be separated from the Na^{23}/Al^{27} interactions. It is therefore apparent that the simple HB-FID does not lend itself as the most suitable approach to uncovering electron-nuclear interactions. However it is still an effect that requires due consideration, since even for low mw powers it has the ability to produce subtle distortions in a field-swept FID-detected spectrum in a manner analogous to the way in which the nuclear modulation effect distorts echo-detected EPR. An example is given in Fig. 9, where lines of maximum modulation due to remotely coupled nuclei follow hyperbolae.[3]

VII. CONCLUSIONS

The primary purpose of this article has been to report a simple phenomenon rather than to introduce a new method or technique per se. We have shown that a hole-burning mw pulse applied to inhomogeneously broadened systems can produce beats in the free-induction signal. This HB-FID yields the superhyperfine frequencies of coupled nuclei with (ideally) the intensity of allowed transitions. We were restricted to rectangular mw pulses but clearly shaped pulses would offer a more ideal excitation profile for these purposes. The qualitative description of the phenomenon is similar to that used to explain the FT-EPR detected NMR experiment and the two have therefore been directly compared. The former relies on the measurable EC following the hole-burning pulse and is limited by T_M relaxation, while the latter utilizes the EP pattern burnt into the EPR line and is therefore effectively limited by $T_1 > T_M$ relaxation. Although the experimental examples shown herein have yielded only interactions with weakly coupled (remote) nuclei, the ideas are equally applicable to any paramagnetic system with hyperfine interactions and a sufficiently large inhomogeneous width.

ACKNOWLEDGMENT

One of the authors (S.C.D.) wishes to acknowledge the financial support of the Monash Graduate Scholarship.

[1] J. A. Coelho Neto and N. V. Vugman, J. Magn. Reson. **125**, 242 (1997).
[2] R. H. Fritsch, P. Höfer, K. Holczer, and D. Schmalbein, in *Electron Magnetic Resonance of Disordered Systems*, edited by N. D. Yordanov (World Scientific, Singapore, 1989), pp. 59–69.
[3] S. C. Drew, J. R. Pilbrow, P. J. Newman, and D. R. MacFarlane, J. Phys. D **34**, 2987 (2001).
[4] Th Wacker and A. Schweiger, Chem. Phys. Lett. **186**, 27 (1991).
[5] S. A. Dzuba, I. V. Borovykh, and A. J. Hoff, J. Magn. Reson. **133**, 286 (1998).
[6] A. Schweiger, L. Braunschweiler, J. M. Fauth, and R. R. Ernst, Phys. Rev. Lett. **54**, 1241 (1985).
[7] L. Braunschweiler, A. Schweiger, J. M. Fauth, and R. R. Ernst, J. Magn. Reson. (1969–1992) **72**, 579 (1987).
[8] S. Nakanishi, O. Tamura, T. Muramoto, and T. Hashi, Opt. Commun. **31**, 344 (1979).
[9] E. Hoffmann and A. Schweiger, Chem. Phys. Lett. **220**, 467 (1994).
[10] M. Willer and A. Schweiger, Chem. Phys. Lett. **230**, 67 (1994).
[11] A. Schweiger and G. Jeschke, *Principles of Pulse Electron Paramagnetic Resonance* (Oxford University Press, New York, 2001).
[12] L. Braunschweiler, A. Schweiger, J. M. Fauth, and R. R. Ernst, J. Magn. Reson. (1969–1992) **64**, 160 (1985).
[13] D. R. MacFarlane, C. R. Bradbury, P. J. Newman, and J. Javornitczky, J. Non-Cryst. Solids **213&214**, 199 (1997).
[14] S. A. Dikanov and Y. D. Tsvetkov, *Electron Spin Echo Envelope Modulation (ESEEM) Spectroscopy* (CRC, Boca Raton, FL, 1992).